Silicon carbide particulates incorporated into microalloyed steel surface using TIG: microstructure and properties

P. Muñoz-Escalona[1], F. Sillars[2], T. Marrocco[2], R. Edgar[3], S. Mridha[4] and *T.N. Baker [4]

[1] School of Computing, Engineering and Built Environment.
Glasgow Caledonian University, Glasgow, G4 0BA

[2] Advanced Materials Research Laboratory
University of Strathclyde, Glasgow, G1 1XJ, UK

[3] Impact Solutions, 16, Abbotsinch Road,
Grangemouth, FK3 9UX

[4] Department of Mechanical and Aerospace Engineering,
University of Strathclyde, Glasgow, G1 1XJ, UK

*Corresponding author

This is a copy of the revised paper for MST including Figures and Tables

ABSTRACT.

Surface metal matrix composites have been developed to enhance properties such as erosion, wear and corrosion of alloys. In this study, ~5 μm or ~75 μm SiC particulates were preplaced on a microalloyed steel. Single track surface zones were melted by a tungsten inert gas torch, and the effect of two heat inputs, 420Jmm^{-1} and 840 Jmm^{-1},compared. The results showed that the samples melted using 420Jmm^{-1} were crack-free. Pin-on-disk wear testing under dry sliding conditions were conducted. The effects of load and sliding velocity were used to characterise the performance of the crack-free samples. Microstructural and X-ray diffraction studies of the surface showed that the SiC had dissolved, and that martensite, was the main phase influencing the hardness.

Keywords: Surface engineering; Microalloyed steel; Silicon carbide particulates; Particle size; TIG melting; Wear rate; Microhardness.

1.Introduction

Surface engineering is an important aspect of several engineering industries and is widely used in additive manufacturing. The surface of a material may have a crucial role in determining the load bearing capacity of a component and ultimately the time in service, and is where problems due to poor resistance to wear and oxidation are encountered [1]. Many of the ideas currently followed for surface alloy compositions were developed from bulk metal matrix composites, (MMC's). As a route to improving the wear resistance of some alloys, silicon carbide has been one of the ceramics of choice for developing bulk MMC's[2]. It has advantages of being hard, available in a wide size range, at various purity levels, and is relatively cheap. Improvements in the wear resistance of MMC's containing SiC particles have been reported in aluminium alloys [3-6]and copper alloys [7].

Coatings, often a few microns in thickness, can improve the surface properties giving a material an extended product life cycle and reduce the risk of failure [6]. However coatings can in some circumstances be detached from the substrate surface. An alternative approach is to modify the surface region of a material by incorporating another chemical species, chosen to mitigate damage during service. For example, ceramic particles were incorporated into the surface of titanium by laser processing, resulting in improved wear and oxidation resistance. This has been undertaken by cladding [8,9] or by the creation of a functionally gradient surface [9,10]. Pioneering work by Ayers and co-workers [11-14] who injected hard particles of TiC or WC into laser surface melted zones on various substrates, demonstrated that with a greater volume of carbide particles, the wear resistance was improved and the coefficient of friction decreased. However, with a SiC addition to a Ti-6Al-4V alloy, a much higher hardness, reaching 1400Hv just below the surface was recorded [15]. This hardness level should have a significant influence on the wear resistance of the modified surface [16].

It is evident from the literature that the development of improved wear resistance through the incorporation of SiC particles to produce MMC's by laser surface engineering is well established for the light alloys aluminium, magnesium and titanium [8-15,17-20].

High tonnage applications based on steels in, for example, civil engineering, mining and transportation industries, require relatively cheap methods of manufacture, developing surfaces with a combination of high strength, toughness and wear resistance. To achieve these properties, an understanding of the influence of microstructure on properties is important.

One of the earliest studies on the effect of an addition of SiC particles on the phases formed in liquid steel was undertaken by Terry and Chinyamakobvu [21]. They found that a rapid reaction occurred forming iron silicides and graphite. Reactions in the matrix and interface of Fe-SiC MMC system were considered by Pelleg [22].

A number of workers have studied surface engineering of steels. Gemelli et al. [23] laser alloyed a pre-deposit of Cr_3C_2 or SiC on a tool steel, which gave excellent oxidation resistance. More recently Čikara et al. [24] produced surface MMC's by adding SiC particles to low or medium carbon steels, while Zhang et al. [25] used a high inductive heating technique to clad 20mm dia., 5mm thick coupons of a medium carbon steel with mixed Ni60-SiC nano powders. In this latter work, XRD spectra taken after cladding, detected no sign of SiC. It was considered that SiC dissolved and dispersed throughout the clad zone.

An improvement in the wear properties of mild steel through laser cladding was achieved by Majumdar et al.[26], who aimed to develop a compositionally gradient SiC dispersed phase. The SiC dissociated and precipitated as Fe_2Si, raising the hardness from 190HV of the mild steel substrate to ~600HV at the surface. The substitution of a laser by a more economical tungsten inert gas (TIG) was initially made by Mridha and Ng [27] for surface engineering of titanium. More recently Buytoz [28] has undertaken TIG processing of steel, studying several different SiC contents and using a range of energy inputs, some resulting in

the dissolution or partial dissolution of SiC particulates. Also Reddy et al. [29] used a TIG torch shielded by argon to incorporate ~50μm size SiC into mild steel. A linear increase in hardness with Si content from that of the mild steel, 160Hv (Si 0.23%), to ~400HV (Si 1.5%) was recorded. In a similar study by Patel et al., [30] ~5μm SiC particulates were dissolved into a microalloyed (MA) steel surface also using a TIG torch, with argon as the shielding gas. A modified surface of hardness >1000Hv to a depth ≥1.4mm was developed. This study was expanded by Muñoz-Escalona et al [31], who found that substituting helium for argon as the shielding gas in single track TIG processing, reduced the melt zone hardness due to the significantly higher temperatures recorded in the parent microalloyed (MA) steel. Changes in heat input, shielding gas, and alloying powder composition, volume fraction and size, can also influence the surface roughness. In many applications, a low surface roughness parameter, Ra, is demanded [32-34]. In other cases, the surface is required to have a machined finish [35,36]. Therefore it is essential that the surface treatment produces a modified layer of such a thickness that it still provides improved wear or erosion resistance over the life-time of the component after machining.

Following preliminary work [37], the present research is a part of a wider study assessing the potential of TIG processing for creating modified surfaces based on powder alloying techniques, to achieve superior wear properties for an MA steel, In particular, the influence of SiC particulate size on the retention of the ceramic and contribution to hardness and abrasive wear properties following TIG processing of an MA steel, were considered.

2.Experimental Procedure

A surface engineering technique based on a TIG torch was used to melt tracks in three MA steel samples, two incorporating SiC of different particulate sizes, ~5 μm or ≤ 75 μm, which were compared with a processed as-received MA steel.

The chemical composition of the MA steel substrate base metal (BM) plates, with the dimensions 300 x 30 x10 mm, and a hardness of ~150Hv. was determined using a Glow Discharge Optical Emission Spectrometer, model Horiba GD-OES profilometer as 0.14C-1.26Mn-0.32Si-0.004S-0.015P- 0.012Cr-0.002Mo-0.007Ni-0.02Cu- 0.028 Al -0.037Nb - 0.008Ti- 0.001V (wt. %). The steel surface was ground on emery paper and degreased in acetone prior to the application of the preplaced powder. Silicon carbide powder of ~5μm or ~75 μm size, at a concentration of 0.3 mg mm^{-2} relative to the area of the steel specimens, was mixed with a binder and preplaced on the BM surface. Details of the powder pre-placement method have been described previously [27]. Dynastry 300DX TIG equipment was used to generate an arc with a 2.4 mm diameter thoriated tungsten electrode. Surface engineered single tracks were compared following TIG processing using initially three energy inputs, 210 J mm^{-1} ,420 J mm^{-1} and 840 J mm^{-1}. Argon was the shielding gas. The temperature during the melting and cooling process was registered by K type thermocouples placed in three 1 mm diameter holes drilled to a depth of 5mm below the surface of the sample to be processed. The three holes divided the sample into 4 equal lengths, and the location of thermocouples is shown in a schematic drawing, Figure 1. Table 1 gives the conditions used in this work.
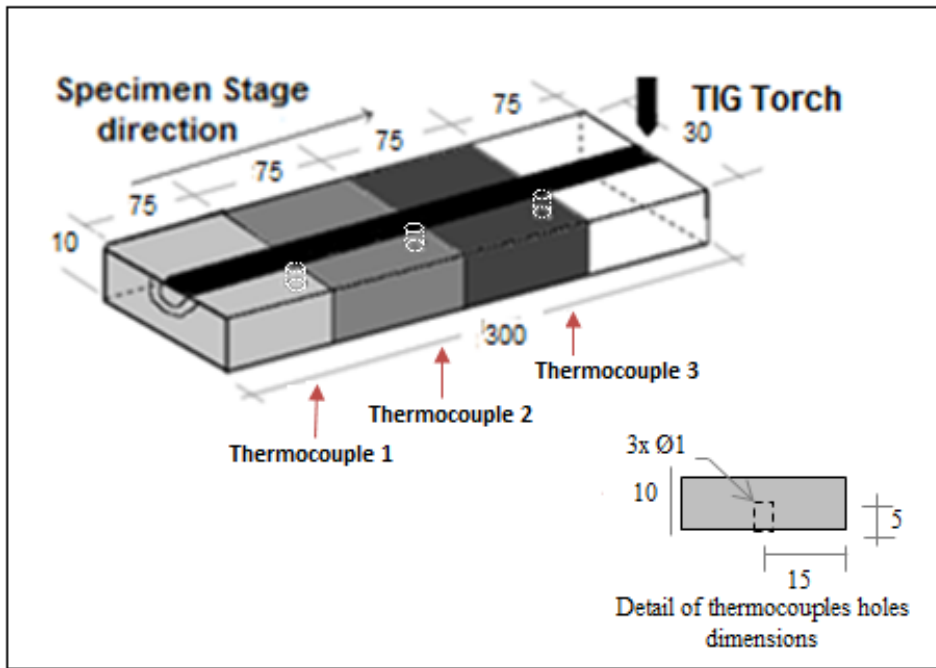
Fig.1. Schematic drawing showing in black the melt track, melting direction and location of three thermocouples.

Table 1. Melting conditions used in the research

Sample	SiC with Particulate size (µm)	I (A)	V (V)	S (mms⁻¹)	E (J mm⁻¹)
1	0	80	11	2	210
2	0	80	11	1	420
3	0	80	11	0.5	840
4	5	80	11	1	420
5	5	100	17	1	840
6	75	80	11	1	420
7	75	100	17	1	840

0 = no SiC ceramic powder added

Table 2 shows different properties of the different materials/elements involved in the work.

Table 2. Density and thermal properties of the microalloyed steel, SiC and argon gas.

Material \\ Property	Mild steel	SiC	Argon
Density [kgm^{-3}]	7870	3210	1.67
Specific heat, c_ρ [kJ Kg K]	0.5	0.75	0.52
Thermal conductivity [Wm^{-1} K^{-1}]	49.8	80(HP)71(sintered) 490(αSiC)	0.016
Specific gravity	7.8	3.2	1.38

The energy input (E) was calculated using Eq. 1.

$$E = \eta \frac{V*I}{S}$$

(1)

V: voltage

I: current

S: velocity

η: efficiency of energy absorption, which was taken as 48% for a TIG process [38].

The temperature of the samples 5mm below the surface was registered during and after processing; the samples cooled to room temperature when a microstructural examination and microhardness measurements were conducted.

Each sample was cut just beyond the location of each thermocouple and prepared metallographically giving a total of three specimens from each sample,75mm apart as observed

in Figure 1.The 20~25 mm of the first section to be processed, before thermocouple 1, was discarded, to ensure that the processing was conducted with a stabilized torch.

A Mitutoyo MVK G1 microhardness tester with 200gf load and a 15s delay was used to record microhardness data to ± 5Hv, following BS 1043-2 1993 and BS6507-1 1998.The cross-sectional area of each sample was measured, starting at 0.1 mm from the fusion zone edge and recording measurements in a vertical distance 2 mm.

Wear tests were undertaken under dry sliding conditions using a pin-on-disc tribometer following ASTM G99 standards. After the TIG processing, pins were cut from the sample between thermocouple positions 2 and 3, ie. between150mm and 225mm from the start of the melt track, which was   also considered to have an optimal outcome regarding cross- sectional area appearance. Each pin was ~5mm dia. and 10mm height, shown schematically in Figure 2.

The positions from which the wear test pins were taken, the specimens for microhardness testing, metallography and for the XRD investigations, were as closely related as possible so that the respective data was relevant; ie. between 125mm and 150mm from the start of TIG processing.
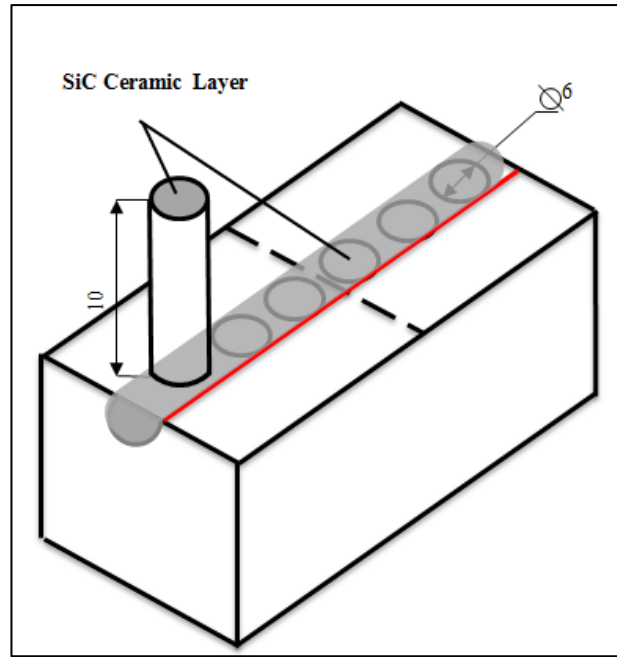
Fig.2. Schematic drawing of the wear test pins taken from the sample between thermocouple positions 2 and 3.

The steel disc counterfaces, with dimensions of 75mm dia. and 3mm thickness, had a chemical composition determined by the GD-OES technique of 1.05C-1.23Mn-0.28Si-0.58Cr-0.27V-0.46W (wt. %), and a mean hardness of 190HV.

The wear loss of the pins of the MA steel without SiC additions and with ~5μm and ~75 μm particulates was recorded after testing under three loads,10, 30 and 50N. A constant sliding distance of 10km was used, which, based on the wear track diameter, equates to ~ 56,000 revs. This sliding distance was selected based on previous research [39]. If the processed surface was fully worn, the test was terminated.

The wear rate W_s and the coefficient of friction, μ, were calculated using equations 2 and 3.

$$W_s = \frac{\Delta V}{F_N L} \qquad (2)$$

W_s: Wear rate, mm³ N⁻¹m⁻¹

ΔV: variation in volume, mm³

F_N: Normal load, N

L: Sliding distance, m

$$F_f = \mu F_N \qquad\qquad (3)$$

F_f: Frictional force, N

μ: Coefficient of Friction

F_N: Normal load, N

To obtain the wear rate W_s, the mass loss from both the pin and the disc were recorded at 5min.intervals, either until the trial had been completed, or until the modified surface had been fully worn. Measurements were taken using a Mettler College balance, which has a readability tolerance of $1x10^{-4}$ g and maximum capacity of 220g.

Specimens were prepared for metallographic analysis following ASTM E3-01 standards. The crystallographic characterization of phases developed in the re-solidified surface was obtained by X-ray diffraction (XRD), which was carried out in a Bruker D8 Advance with Da Vinci. A Cu ($\lambda = 1.5406$ Å) source x-ray tube was used. The x-ray tube was set to 40kV and 40mA, the step size of 0.02º and the dwell time of 0.5s. The 2-theta range measured was 20 -90º. XRD data from all these sources was characterized using the International Centre for Diffraction Data (ICDD) PDF-2 database incorporated in the XRD equipment, also allowing indexing of many of the peaks. However, with such a complex mixture, the individual phases were only tentatively identified by their peak 2θ values, which did not always give the expected peak heights and widths, as required by a Reitveld refinement, suggesting that some peaks are multiples.

 XRD spectra were recorded for MA steel samples with ~5µm and ~75µm SiC particulate additions from the melt zone(MZ) surface from between thermocouples 1 and 2, to study the

phases as a function of particulate size. In addition, XRD spectra where collected from the BM in the as received condition, also after heating to 600°C for 30 min to stress relieve the surface engineered steel, and from the ~5μm and ~75μm SiC powder samples. A slit size of 200μm was used to limit the XRD information collected to the centre of the ~4mm TIG track width.

An Olympus GX51 optical microscope(OM) and a Hitachi Su-6600 scanning electron microscope (SEM) with an Oxford Instruments INCA system with 80 mm XMAX SDD detector and a wavelength detector were used to record and chemically analyse the microstructure of the metallographic specimens. A Philips TEM 400 fitted with an Oxford INCA system was used to examine carbon extraction replicas.

3. Results
3.1 Temperatures

All the TIG samples recorded a higher temperature at the end of the melted track registered by thermocouple 3, the position of which is shown in Figure 1; this is due to the preheating effect the samples were subjected to during the melting of the track [40]; the difference in temperature between thermocouples 1 and 3 was ~45°C.

Figure 3 shows the maximum temperature registered in the melted track for each of the samples processed under the different energy inputs. An increase in the temperature of ~60% was noted by thermocouple 3 when the energy input was increased by 100% (from 210 J mm^{-1} to 420 J mm^{-1} or from 420 Jmm^{-1} to 840 J mm^{-1}).
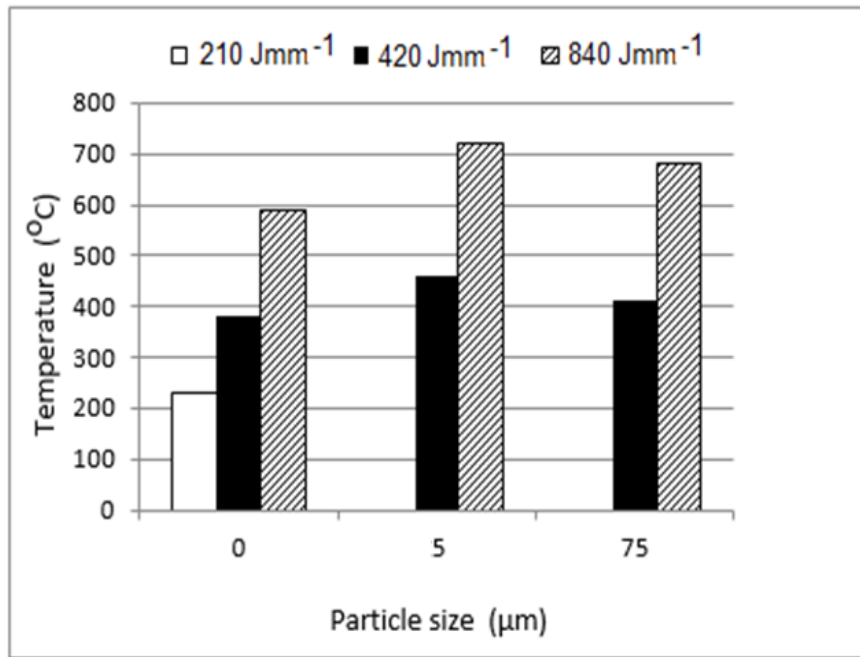
Fig.3. Maximum temperatures registered in the melted zone for each sample, which was by thermocouple 3.

It is also observed that the samples incorporating ~75μm SiC particulates recorded slightly lower temperatures than those with 5μm SiC. This is possibly associated with the greater volume of liquid produced, leading to a larger volume of melt zone. Figure 4 shows that as the energy input was increased from 210 to 840 J mm^{-1}, ie.by 400%, the melted track depth increased by ~60% and the width by~45%. During the determination of the width and depth data it became apparent that an energy input of 210 J mm^{-1} was insufficient to produce a surface capable of incorporating the SiC particulates. As a result it was decided to limit the study at this point to two energy inputs,420 Jmm^{-1} and 840 J mm^{-1}.
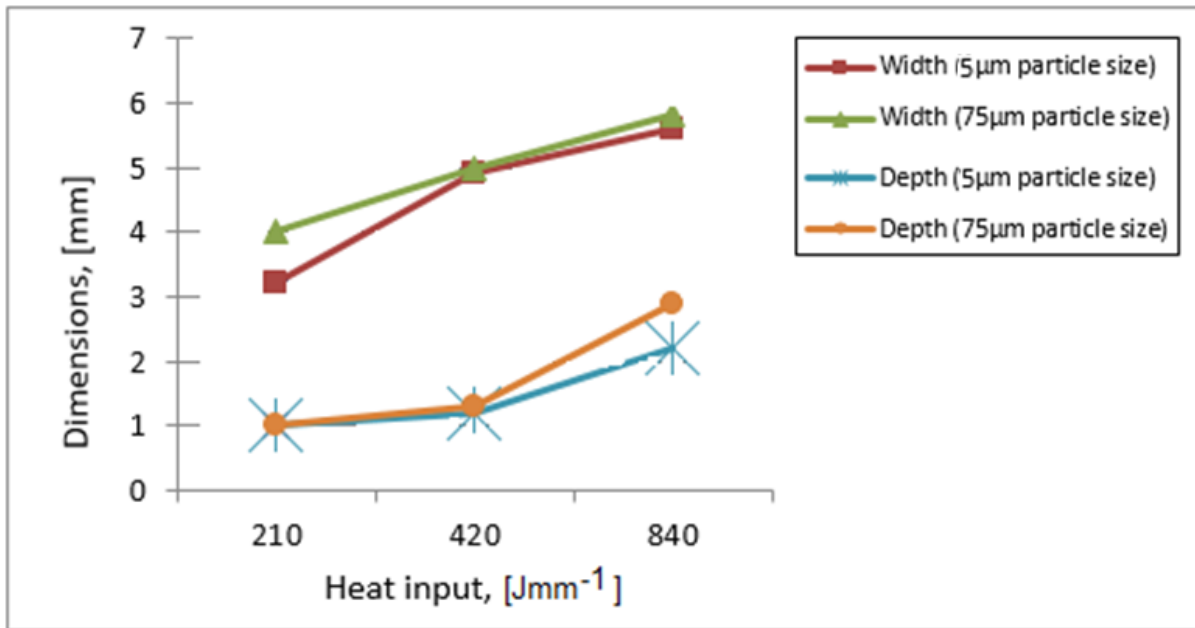
Fig.4. Influence of heat input on the dimensions of the melted zone.

3.2 Microhardness results

Hardness profiles from indents made in the centre of the melt zone, from close to the surface to the BM of tracks processed at $420Jmm^{-1}$ and $840Jmm^{-1}$,are shown in Figure 5, for all the samples. The hardness of the BM steel was ~150HV, which after TIG processing increased to between 220 and 270 HV. Those specimens with SiC additions processed at $420Jmm^{-1}$ and $840Jmm^{-1}$ showed substantial increases in hardness to 800-900Hv, retained for a melt-zone depth >1mm.

Figure 5 near here
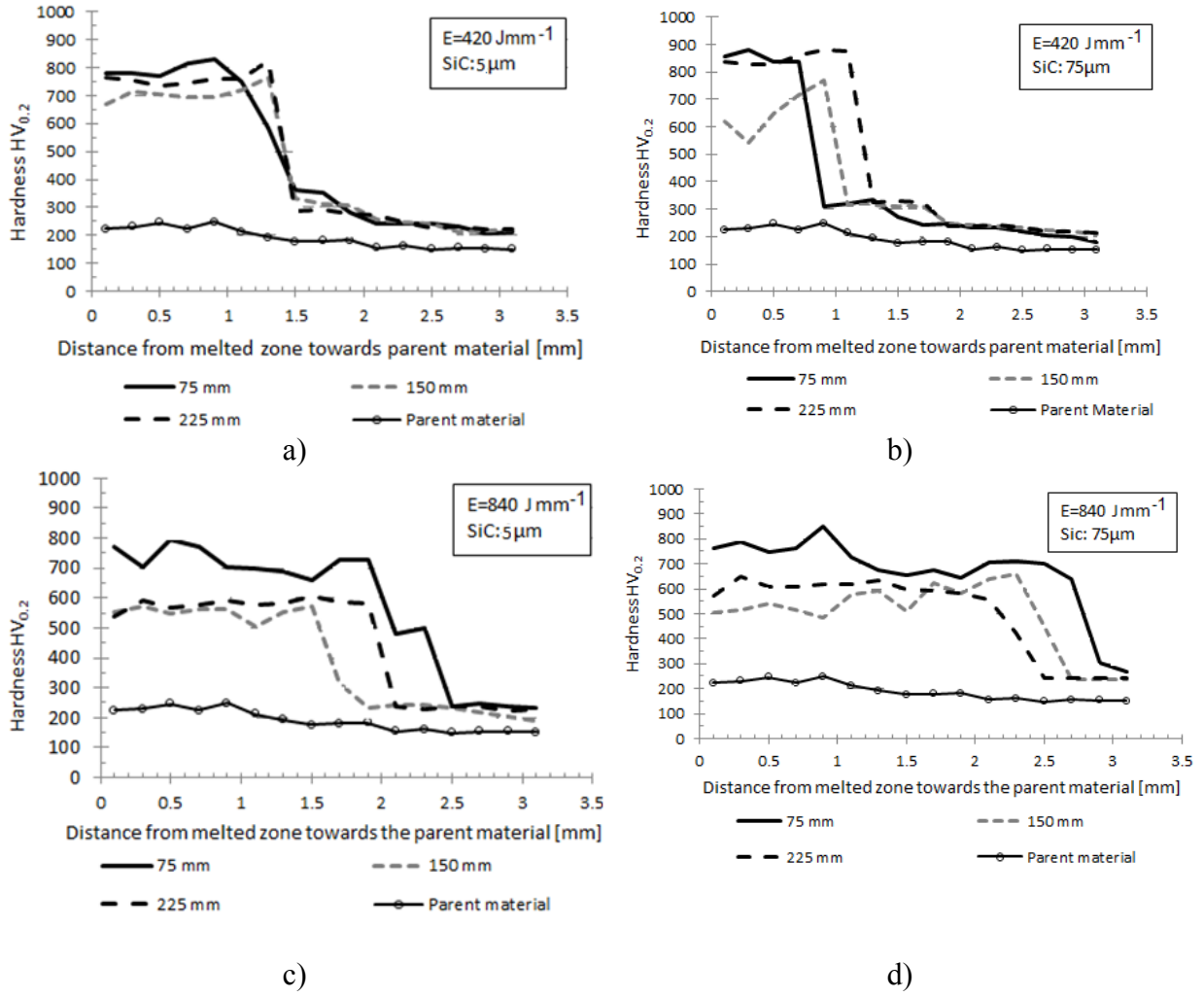
Fig.5. Hardness profile of cross- sectional area at 75, 150 and 225 mm from sample's edge a) 420 Jmm^{-1} (~5µm), b) 420Jmm^{-1} (~75µm) c) 840 Jmm^{-1} (~5µm), d) 840Jmm^{-1} (~75µm).

3.3 Macrographs

Optical Macrographs (OM) of two cross- sections taken from samples at 225 mm along the track are shown in Figure 6. Following TIG processing at 420 Jmm^{-1}, the sample with ~5µm SiC particulates shows no cracks, Figure 6(a), while the cross-section of the track processed using 840 Jmm^{-1} Figure 6(b) shows a shows a significant crack. The same occurred for the samples prepared with ~75µm SiC powder. Despite the greater melt zone volume produced using 840 Jmm^{-1}, it was decided to confine subsequent processing to an energy input of 420 Jmm^{-1}.
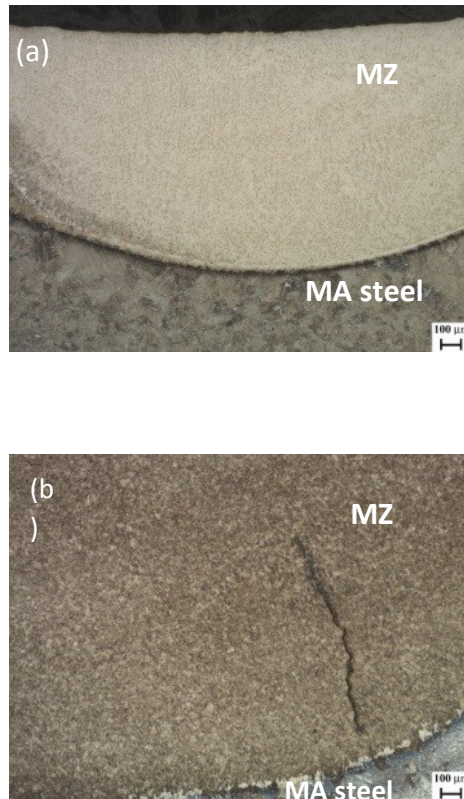
Fig.6. OM showing the melt zone (MZ) and Micro-alloyed steel (MA steel) for 75μm SiC sample at 225 mm: 420 Jmm^{-1}, no cracks (b) 840 Jmm^{-1}, containing an ~1mm long crack.

Figure 7 is an OM from the first and final sections of the TIG processed track.There are marked differences at each end for the two specimens incorporating SiC particulates.For this reason,the following sections reporting a more detailed microstructural charaterization were restricted to the section of the track between thermocouples 1 and 2, but close to 2.Figure2.
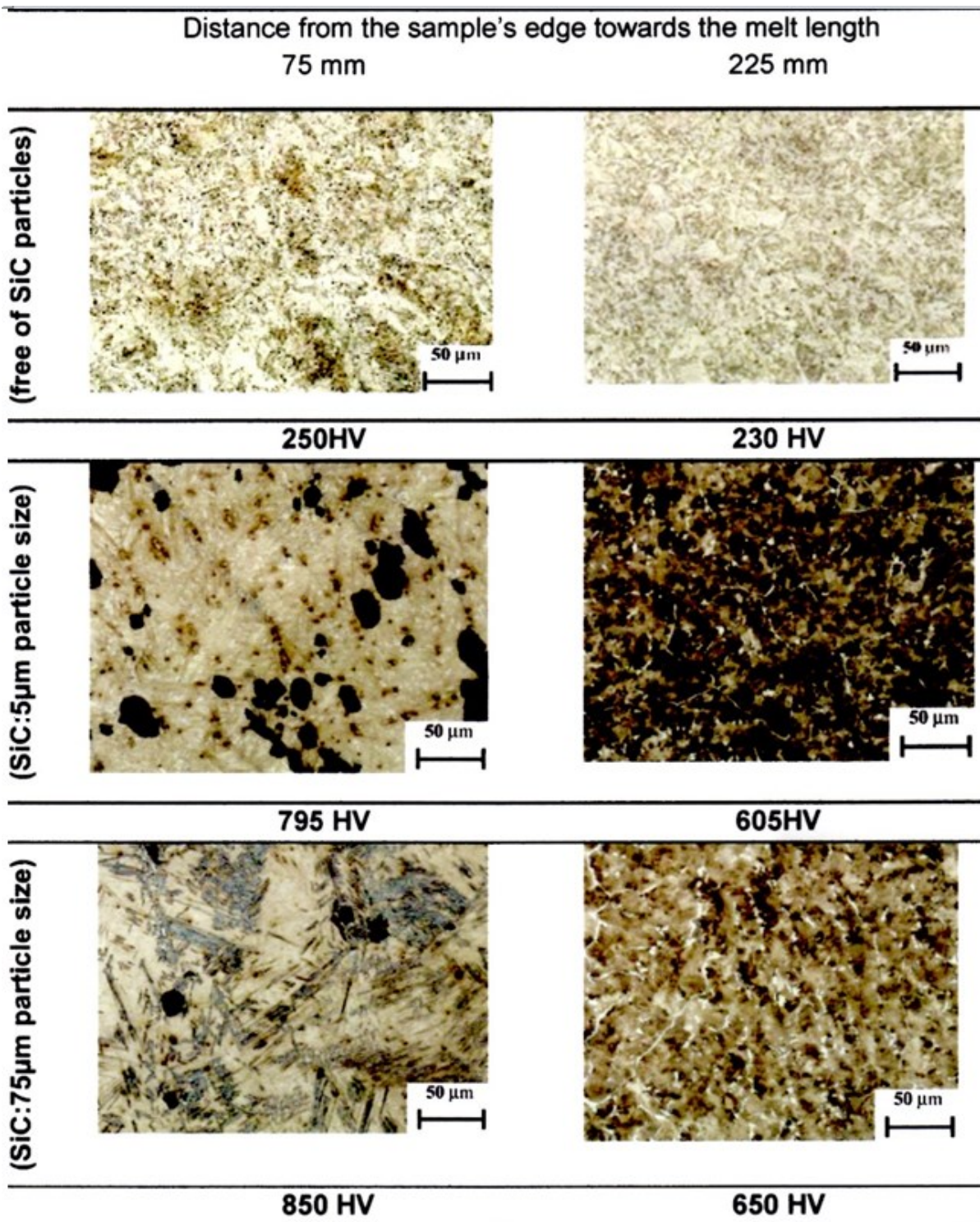
Fig.7. OM of the fusion zone at the start and end of the melted track.

The corresponding microhardness is   taken from Figure 5.

3.4 Wear test results

The test samples, machined from the positions shown in Figure 2 were left un-

groun, to avoid removing any of the region melted by the TIG surface engineering. Therefore

some surfaces were slightly uneven, and a longer running in period during wear testing was
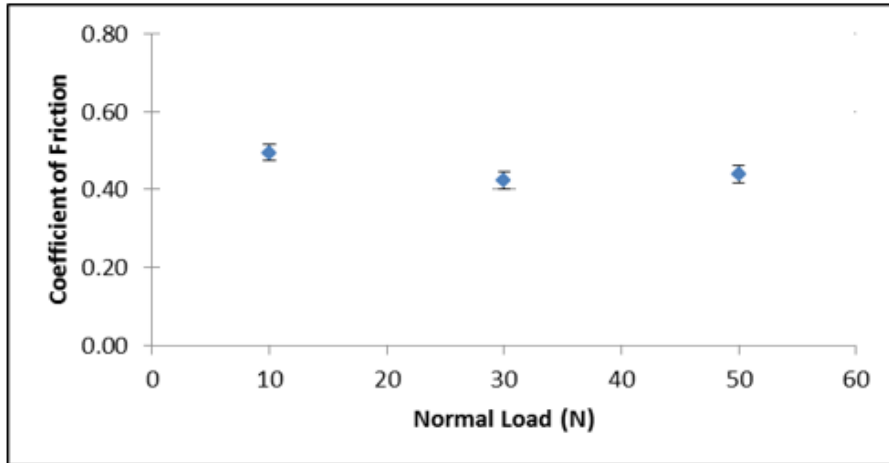
taken for all pins, which is not included in the data plotted in Figure8.

Fig.8.   Influence of normal load on the mean coefficient of friction on samples melted with an
energy input of 420 J mm^{-1}.

Figure 8 shows that loads in the range 10 to 50 N, with a narrow range of test velocities, have

relatively little influence on the coefficient of friction of the samples with an energy input of

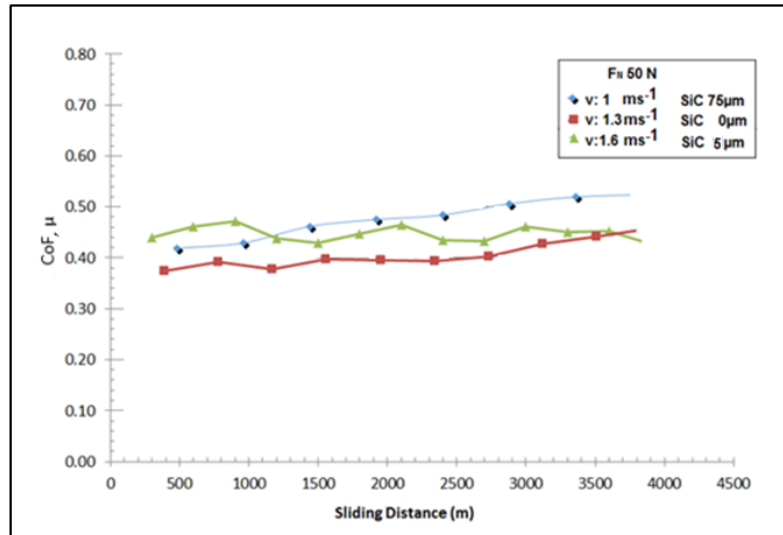420 J mm^{-1} and hence in further work considered only the highest load,50N.

Fig.9. Comparison of coefficient of friction as a function of sliding distance for three samples tested with a load of 50N.

In Figure 9, the CoF of the two specimens incorporating SiC particulates is compared with the SiC-free specimen. This specimen, which has the lowest CoF (red) while the specimen absorbing the largest SiC,~75μm, shows the highest CoF (blue).Both these graphs increase steadily with sliding distance, while the data for the surface coated with ~5μm SiC particulates oscillates ~25% of the mean CoF.There was EDX evidence of a transfer of material from the pin to the counterface during testing, indicated by higher silicon contents on the disc wear tracks than in the untested areas.

3.5 XRD and Analytical SEM results

XRD spectra were recorded for the TIG processed rough MZ surface of the MA steel samples incorporating ~5μm or ~75μm SiC particulates taken between thermocouples 1 and 2, to study the phases developed as a function of particulate size.

The XRD spectrum in Figure 10, collected from the MA steel incorporating ~5μm SiC particulates, shows peaks related to martensite, silicon dioxide, cementite (Cohenite,Fe_3C) and iron silicide (DO_3,Fe_3Si.). With the exception of the austenite peaks, and with the addition of peaks corresponding to graphite, the ~75μm SiC MA steel spectrum contains the same peaks.

Also in Figure 10, spectra are included from the ~ 75µm SiC powder used in this work and from the BM. The strongest peaks excited by the 75µm SiC powder are indicated at 2θ values of ~35°. However, it is apparent that there is insufficient matching between the SiC peaks in the spectrum from the powder alone and the spectra from the TIG processed MA steel/SiC specimens to claim that SiC is present in these latter spectra.

The PDF files used for the identification of these phases are given in Table3.

Table 3. PDF files chosen for the identification of the above phases

Phase		Powder Diffraction File Number
Austenite	(γ)	00-023-0298
Graphite	(G)	00-023-0064
Martensite	(α')	00-044-1290
Fe_3Si	(F)	01-072-4250
SiO_2	(S)	00-046-1242
Fe_3C	(θ)	00-003-0411
Ferrite	(α)	00-006-0696
SiC		00-001-1118

A slight shift appears between some peaks in the spectra of steels with~5µm and ~75µm SiC additions, particularly noticeable at low 2θ values. To investigate if this was due to residual stress introduced during the cooling from the TIG processing, XRD spectra collected from the BM in the as- received condition together with spectra from the MA steel with SiC particulate additions, were compared with spectra obtained after heating the BM to 600°C for 30 min to stress relieve the surface engineered steel. No significant peak shifts were recorded. Due to the complex nature of the MA ~5µm and MA ~75µm spectra in Figure 10, it was considered inappropriate at this stage to apply a Rietveld structure refinement.
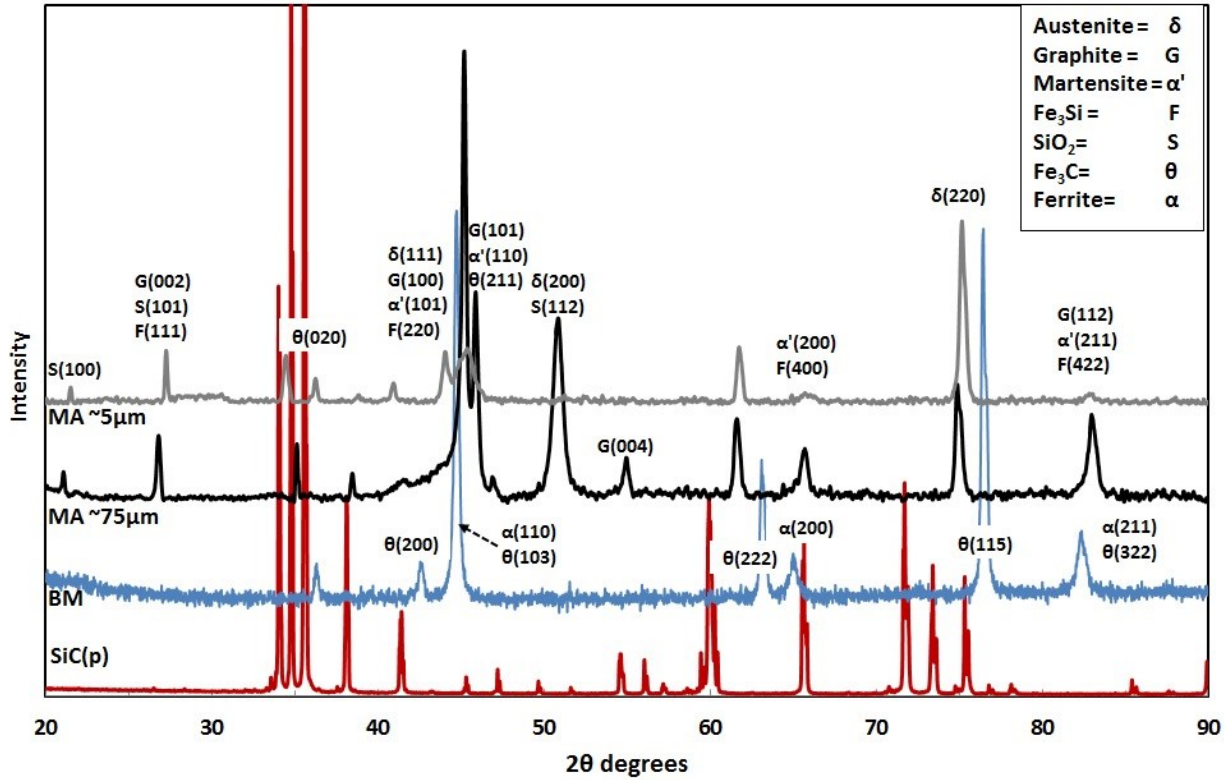
Fig.10. XRD spectra of 75 μm SiC(p), BM, and MA steels with ~75μm SiC and~5μm SiC.

ʼ

The surfaces of TIG processed tracks between thermocouples 1 and 2 are seen in the micrographs in Figures 11a and 11b.Curved ripples following the lines between X and Y are a well- established feature on the surfaces of welded metals which some regard to be entirely due to oscillatory Marangoni flow of the weld pool [41,42]. Figure 11b shows that the track has solidified in a microstructure of fine ridges a-b, which could influence the wear properties of the surface.
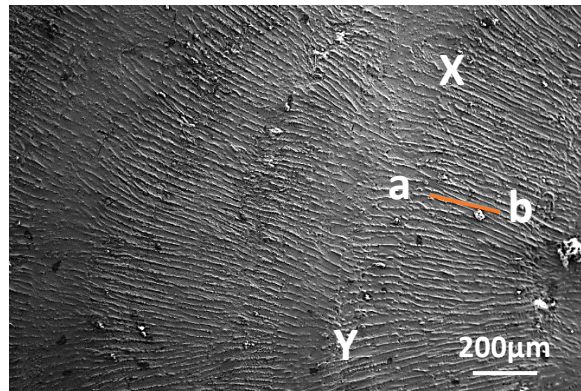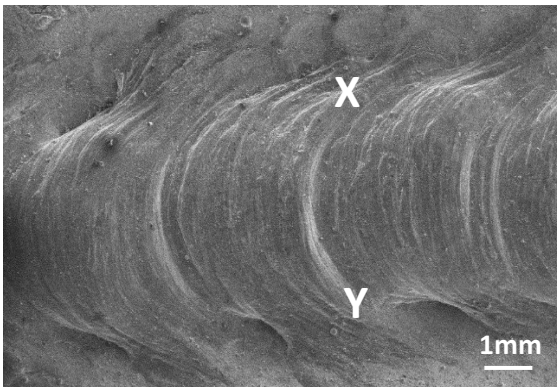
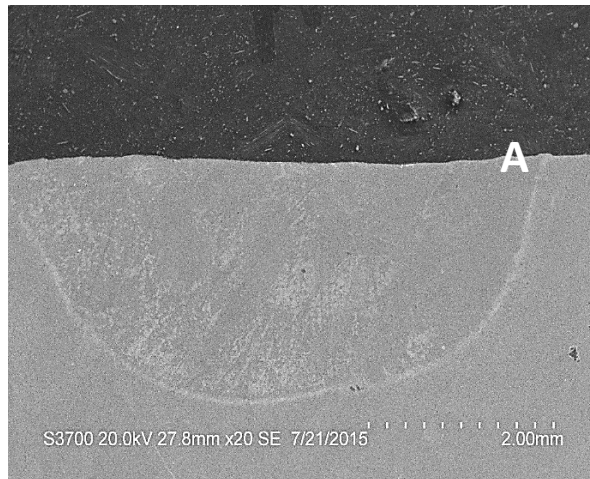**Fig.11a.** SEM micrograph of melt track of ridges ~5µmSiC showing curved ripples, such as XY.

Fig. 11b SEM micrograph showing solidification a-b at ~ 90° to ripple XY

Fig.12a. SEM micrograph of a cross-section of the MZ of ~5µmSiC

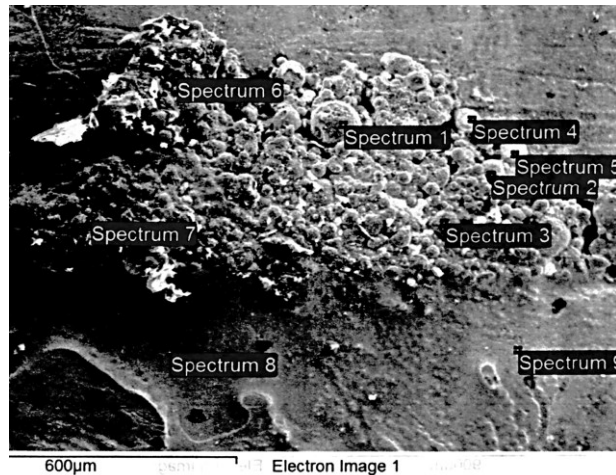**Fig.12b** SEM micrograph of ~5µmSiC un- incorporated phases at A in Fig 12a

Table 4 EDX compositional data corresponding to the nine positions around A indicated in Figure12b

Spectrum	C	N	O	Na	Al	Si	Ca	Mn	Fe	Zn
1	32.3	9.14	8.79	0.42		38.15	0.23	1.11	9.86	
2	26.5		3.83			66.04			3.36	
3	32.58		15.91	0.74	0.39	29.26	2.09	7.18	10.18	1.67
4	43.04		10.48			44.78			1.7	
5	19.56		1.97			73.1			5.37	
6	5.1		1.53			5.31		8.52	79.53	
7	44.43		6.4	0.4		6.74		1.06	40.98	
8	7.93		7.02			5.6		1.08	77.65	
9	15.29		4.01			4.7		1.62	74.37	

Figure12a shows the transverse cross-section of the melt zone while Figure 12b is a higher magnification of area A in Figure 12a. It can be seen that at the edge of the track, following melting and spheroidization, some of the ~5 µm SiC particulates have agglomerated into larger morphologies. Due to the significant difference in density between iron and silicon carbide, Table 2, several agglomerates floated on the liquid steel surface coming to rest at the edge of the

track, but remained on the surface, undissolved in the steel. Most of this discarded particulate would be incorporated in the melt zone when overlapping tracks were used to surface engineer an area.

The EDX compositional data corresponding to the nine positions identified in Figure 12b, is presented in Table 4. Data from spectra 2,4 and 5 suggest the particles are predominantly SiC. This data may also indicate the presence of SiO_2 and an S-C-O phase. Spectra 1 and 3 in Table 4 could be mixtures oxides with some SiC, while 6 to 9 do not fit any single phase.
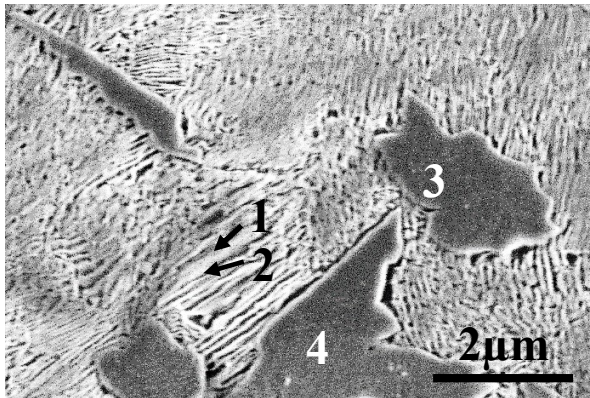

Fig.13a. SEM image of eutectic phase, 1, 2, with unidentified phases, 3,4, in the transverse cross-section of MZ of the MA ~5μm SiC steel.
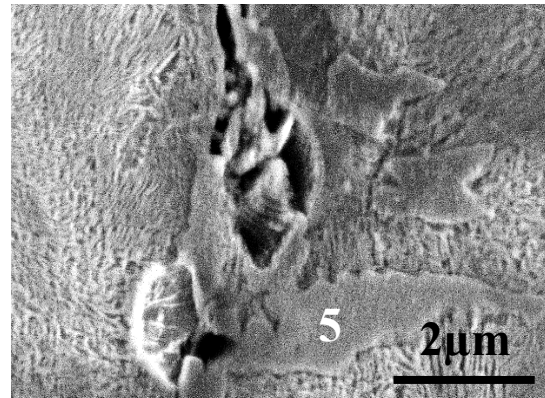

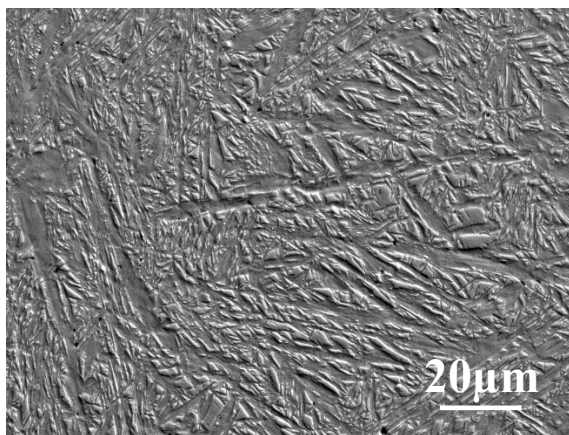**Fig.13b.** SEM image of eutectic phase with a dendritic phase 5

Fig.13c. Low magnification SEM SE image from the surface of the MA steel incorporating ~5μm SiC particulates.
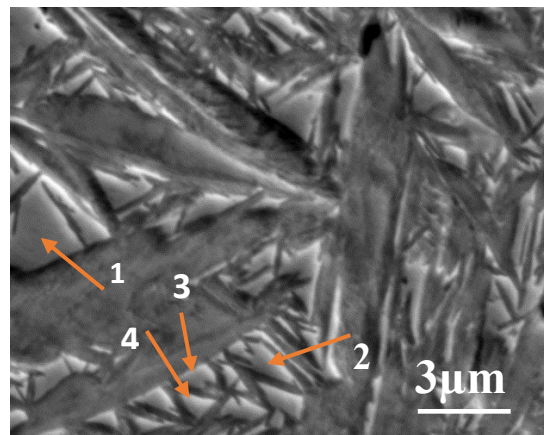

Fig 13d. A second area at a higher magnification with four analytical positions indicated with the corresponding data given in Table 5.

In some regions of the MZ of both SiC incorporated steels, a eutectic phase such as that observed in Figure 13a at 1and 2 for the MA steel with 5µm SiC addition was present, often together with morphologies like 3 and 4, with curved boundaries, and dendritic shapes as at 5 in Figure 13b,which could have formed from the liquid state.

A needle array is observed in the MZ surfaces of both the SiC incorporated steels, Figures 13c, and 13d, (for the MA steel with ~5µm SiC addition), but no graphite nodules were found. This is confirmed in Table 5 for the steel with the ~5µm SiC addition, where the carbon and silicon levels are those recorded throughout the MZ, after TIG processing.

Table 5 EDX compositional data corresponding to the four positions indicated in Fig.13d for the steel with the ~5µm SiC addition

Spectrum	C	O	Si	Mn	Fe	Total
1	5.55	1.21	2.15	1.19	89.91	100.00
2	8.20	3.67	2.18	1.15	84.81	100.00
3	7.92	3.42	1.86	1.15	85.66	100.00
4	6.76	2.52	1.91	1.11	87.69	100.00

A detailed SEM examination of the ~5 µm SiC addition specimen across the surface region to a depth of 500µm, showed that needles were a predominant microstructural feature, with some eutectic phase, an unidentified phase such as that in Fig. 13a and Fig. 13b, (3 to 5), and graphite. The needles are considered to be martensite, as found in the XRD spectra, Figure 10.
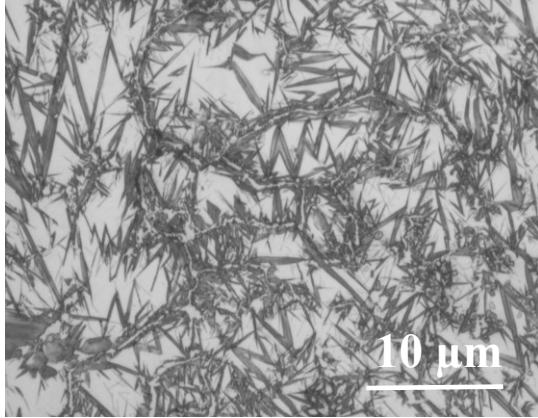
Fig.14a. OM ~75μm SiC MZ top surface showing needles restrained by the boundary phase.
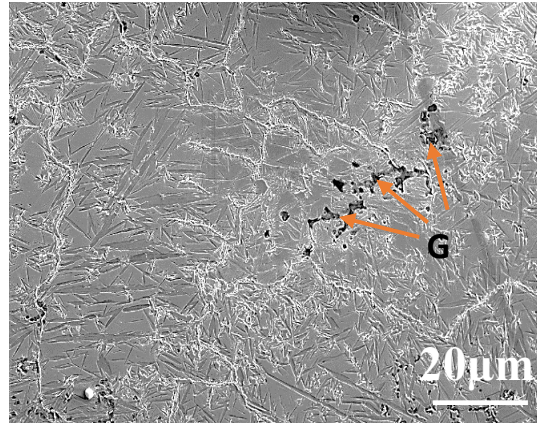

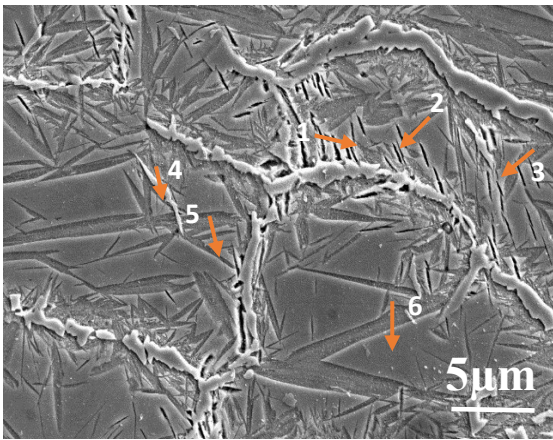**Fig.14b.** SEM ~75μm SiC MZ top surface where G indicates graphite nodules.

Fig.14c. SEM micrograph of ~75μm MZ top surface indicating the positions from which spectra, data in Table 5, were taken**.**
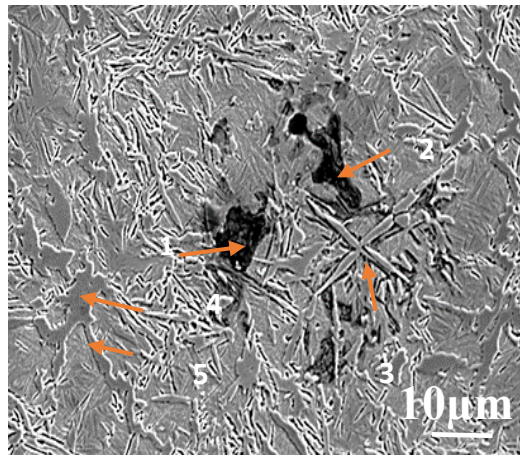
Fig.14d. SEM micrograph of ~75μm MZ top indicating the positions from which spectra, data in Table 6, were taken.

Table 6. EDX compositional data corresponding to the four positions indicated in Fig.14c

Spectrum	C	Si	Mn	Fe
1	3.35	1.73	1.24	93.67
2	5.39	2.84	1.19	90.58
3	10.05	3.80	0.98	85.18
4	6.93	3.19	1.00	88.88
5	6.02	3.21	0.90	89.86
6	6.82	3.55	1.10	88.53

Table 7. EDX compositional data corresponding to the four positions indicated in Fig.14d

Spectrum	C	O	Si	P	S	Mn	Fe
1	60.40	22.10	1.85		0.30	0.73	14.62
2	69.01	5.07	1.28			0.91	23.74
3	6.11	2.47	2.94			1.13	87.35
4	10.57		2.63	0.73		3.98	82.09
5	6.82		3.80			1.32	88.06

The micrographs in Figures 14a to 14d are from the transverse section of the MZ of the ~75µm SiC MA steels, showing some similar needle features to those in Figures 13c and 13d, observed in the steel with a ~5µm SiC addition. Figures 14c and 14d are two SEM micrographs from different parts of the top surface of the MZ of the ~75µm SiC processed specimen, with the corresponding EDX compositional data given in Tables 6 and 7.The carbon levels are overstated and are only included for comparison purposes. Higher carbon levels found for spectrum 1 and 2, Table7, are associated with the black nodules seen in Figure 14d.They are considered to correspond to graphite detected by XRD, Figure 10. Silicon is known to promote the formation of graphite.

Figure 15a is a bright field TEM image of the only type of particles extracted onto carbon replicas from the MA steel incorporating ~75µm SiC particulates. The SAED pattern, Figure15b is indexed as hcp [0001], a=0.4913nm, c=0.5405nm, quartz (silicon dioxide). This is in reasonable agreement with the EDX spectrum, Figure15c, which gave a main chemical analysis of 0%C-2 % Fe-9%Al-33%Si-46%O.
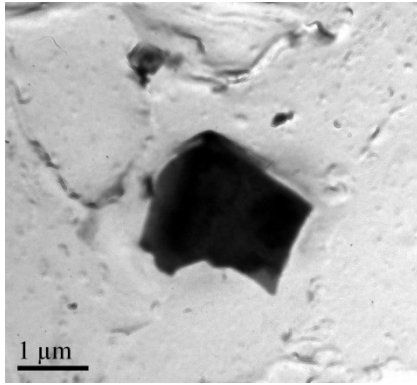
Fig. 15a. TEM bright field image from ~75µm SiC specimen of a particle on extracted on to a carbon replica.
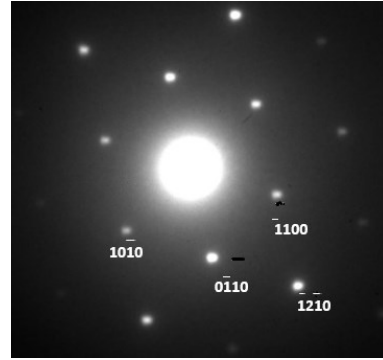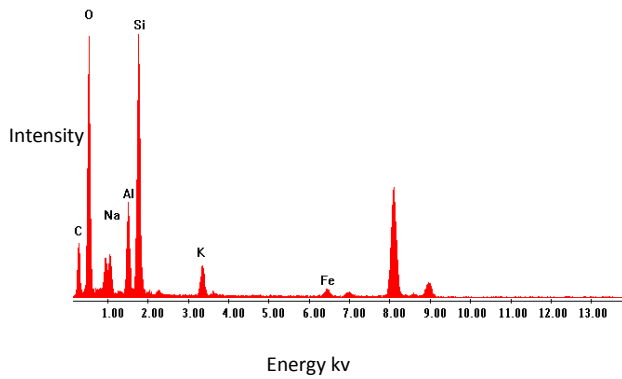

Fig.15b. SAED of particle in Fig.15a.

Fig.15c. EDX spectrum of particle in Fig15 a.

4.Discussion

This research had the aim of exploring the effect of SiC particle size on the wear behaviour of a TIG processed microalloyed steel. It was anticipated that most of the ~75µm SiC addition would remain undissolved following the comparatively low 420Jmm[-1] energy input, but might be more prone to dissolution into the BM matrix with an energy input of 840 Jmm[-1]. Only after the microstructural examination by analytical SEM and TEM, together with XRD spectra analysis, which showed no series of peaks corresponding to SiC, was it apparent that both sizes of the SiC particulates had dissolved, raising the levels of both carbon and silicon in the iron matrix. Dissolution of SiC powders have been reported in titanium alloys [17] and

nickel [43]. Others had reported mainly partial dissolution in steels [22,24,25]. However, in the present work, substantial increases in the microhardness were recorded. Initially, this result was not entirely unexpected, as previous work with lasers and TIG employing higher energy inputs than the present work but with similar volumes of SiC powder, reported SiC particles along with iron silicides, contributing to an increased hardness [26,28-31].

The influence of the energy input on the maximum temperatures recorded for the TIG processed samples is shown in Figure.3. The energy input of 210 J mm^{-1}is included for comparison, but the low temperature recorded by the thermocouples was an indication of the surface temperature being too low to produce a melt capable of incorporating the SiC particulates. An increase in the temperature of ~60% was noted when the energy input was raised by 100% (from 210 J mm^{-1} to 420 J mm^{-1} or from 420 Jmm^{-1} to 840 J mm^{-1}), which did produce a suitable molten track. The dimensions of the melt zones are given in Figure 4. These results are broadly in agreement with previous research by Buytoz [28] and Tewari et al. [44], who highlighted the influence of the processing parameters on the fusion zone dimensions. Figure.4 shows that the melt-zone depth of the steels with SiC particulate additions increased with an input energy of 420 Jmm^{-1}, and significantly using 840 Jmm^{-1}.

The variation of microhardness for all the specimens is shown in Figures 5a to 5d.

Figure 5(a) shows little difference in the maximum hardness for the three positions 75mm, 150mm and 225mm, along the track after processing at 420 Jmm^{-1},which was retained to a similar depth. With the 75 μm SiC specimen, the hardness is retained to >1mm only for the 225mm section, Figure 5(b).

Following processing at 840 Jmm^{-1}, where the cooling rate would be slower than after 420 Jmm^{-1} processing, as expected, lower values of hardness are recorded. However, hardness levels of >650Hv were achieved to a depth of ≥ 2mm in the 75mm tracks, but were lower ,<600Hv, at 150mm and 225mm,Figures 5(c) and 5(d). Figure 3 shows that the temperature recorded 5mm

below the surface indicated little difference for each energy input between the two steels with SiC, which would be expected to reflect similar temperatures of the melt zones. However, Figure 4 shows that the energy input of 840Jmm^{-1}developed a significantly larger melt zone, and it is this which is considered to be associated with the cracking observed in Figure 6. This resulted in the energy input of 420 Jmm^{-1} being used for the next stages of the work.

Figure 5 shows that the hardness of the BM as –received MA steel was ~150Hv. Without any SiC addition, this increased by the TIG processing to 200-270Hv, which is that predicted for a ~0.1%C MA steel. However, the two steels with SiC additions show substantial increases in hardness of >3x the TIG processed BM steel-plate, Figures.5a and Figures.5c where it can be observed that a slightly higher hardness was achieved for ~5μm particles and higher values of hardness were reported for the lower energy input,420 Jmm^{-1}, sample.

The wear rates for the samples incorporating the ~75 μm SiC particulates, collated in Table 5, 2.0,1.0,1.3 x10^{-9} mm^3 Nm^{-1} in order of increasing load, are significantly lower compared to those for the ~5μmSiC sample, 6.7,25,18, x10^{-9} mm^3 Nm^{-1}.In fact, the latter show little improvement over the two tests on the parent steel substrate, 23 and 15 x10^{-9} mm^3 Nm^{-1}.

The microhardness data is an average of that conferred by the components of the microstructure. However, in terms of the wear resistance, the hardest component here is SiC, ~2000Hv. The SiC powder which possibly floated to the edge of the molten track, Figure 12b, but was not incorporated into the melt zone, was not found in the XRD spectra from the as-TIG processed surface, Figure 10. The XRD slits were adjusted to a width of 200μm to include only the centre region of the melt zone track, which explains why the SiC particulate observed in Figure 12b did not contribute to the MA steel spectra in Figure 10.

All the tracks from which the wear pins were machined, Figure2, were processed at an energy input of 420 Jmm^{-1} and taken from the steel between thermocouples 2 and 3. Figure 9 allows a comparison of the change in the CoF with sliding distance for two specimens which

incorporated SiC particles with the untreated specimen. It is evident that the specimens with no SiC addition have the lowest CoF range,0.38 -0.44 (red), which is within the range of data given in the literature for low carbon steels [45]. The graphs of the steels without SiC addition and with ~75μm SiC increase steadily with sliding distance, with the latter recording the highest CoF (blue). By comparison, the data for the surface coated with ~5μm SiC particulates oscillates ~25% of the mean CoF.The increase in CoF with increasing sliding distance was not expected, nor was it in agreement with the investigation of Daoud and Abou El-khair [4] or the laser processing of Ayers et al [11-14].This result could be associated with the absence of SiC particulates in the surface regions of both the TIG processed MA/SiC steels. It may also be that the surface roughness, which was not possible to record in this work, has influenced the CoF during wear testing, rather more than the surface microstructure.

The rippled surface of the steels after incorporation of SiC particulates is shown in Figures12a and 12b. Ripples have been observed in the surfaces of welded metals [41,42], MA steels surfaces modified by pulsed TIG [46] and laser surface engineered titanium [47]. They are considered to be due entirely to oscillatory Marangoni flow of the weld pool [41]. Previous research [43] reported that some surface rippling was associated with porosity and cracks; this was not observed in the present work. In many cases, rippling is of minor importance. However, if the amplitude of the ripples is excessive, it may have an effect on surface roughness. This can be important in controlling the wear resistance of some components and is mentioned in a recent review on additive manufacturing [48]

Many compounds have been identified in research concerned with SiC mixing with iron or low carbon steels. Compounds of the iron silicides in the Fe-Si binary system have been noted through XRD spectra. Tang et al [49], who studied the solid state reaction zone between silicon carbide and iron in the temperature range from 1073 to 1373K, mentioned that there exist several iron silicides in the Fe-Si binary system such as Fe_3Si, Fe_5Si_3, FeSi and $FeSi_2$.However,

in the present work, with the exception of the Si% given in Table 4, the usual level was in the range 1.2 to 4 wt%, recorded in the examples shown in Tables 5 to 7. This is between 4-12 times greater than the level of 0.32wt%Si in the BM. The carbon levels recorded by EDX can only be regarded as a guide, but also increased from the BM by the dissolution of SiC during TIG processing, and might be expected to be increased from 0.14%C in the BM by similar figures to silicon.

Based on the range of matrix compositions obtained by EDX analyses in the present work, the Fe-C-Si equilibrium ternary section at 1723K [50], indicates that for a composition at A in Figure16 , the MZ should be a mixture of liquid steel and graphite.
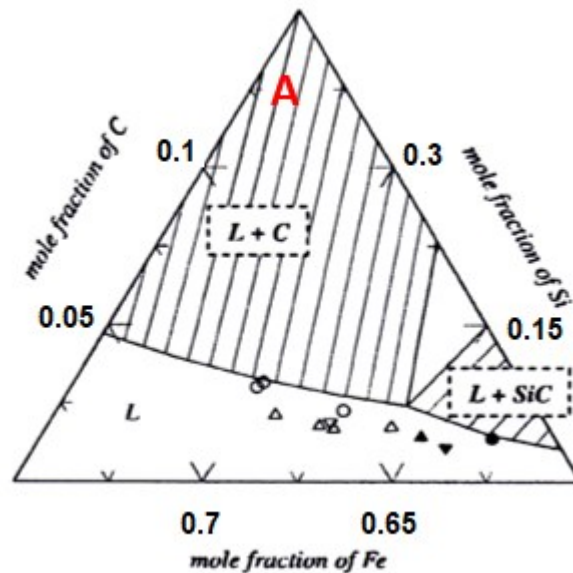

Fig.16. Equilibrium Phase Relationship between SiC and a Liquid Phase in the Fe-Si-C System at 1723K, showing the position at A of the composition in the MZ for the EDAX analyses taken from this work, after Kawanishi et al.[50].

XRD spectra in Figure 10 indicated the presence of graphite in the surface of the steel incorporating ~75μm SiC particulates. Graphite nodules were observed in greater volumes at the edge of the MZ. Also carbon levels of~60wt % in Table7 were recorded from the dark nodules 1 and 2 observed in Figures 14b and 14d. As a result of this information, the dark nodules are considered to be essentially graphite.

Figure 17 is a section of the Fe-C-2%Si equilibrium phase diagram, where the blue line shows a carbon level close to that just necessary for the development of graphite with a silicon content similar to that found in the MZ of this work. The corresponding carbon level in Figure 17 is ~3.9%, which is at the bottom end of the range of 3 to 6wt% EDX levels shown in Table 6, and similar to many other carbon analyses obtained in this research. However, it should be noted that a BM carbon level of 0.14wt % was determined by a Glow Discharge Optical Emission Spectrometer, and that accurate EDX carbon and oxygen data from steels is well established as requiring very stringent specimen preparation and acquisition conditions [51,52].
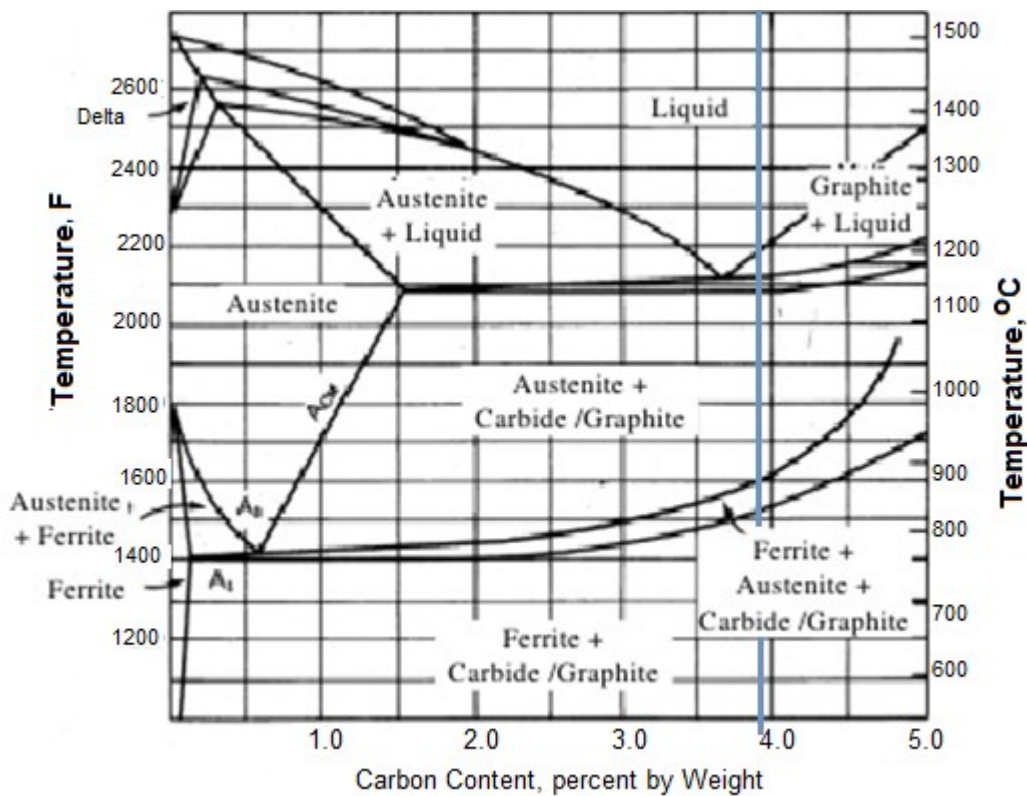

Fig. 17. From the section of the Fe-C-2%Si equilibrium phase diagram.[From SAE]

Cooling the Fe-C-2%Si alloy shown in Figure 17 from the liquid phase, following the blue line at ~3.9wt.% C, predicts that graphite/carbide is formed, and at lower temperatures, the liquid phase solidifies to austenite interspersed with graphite. In the present work, the cooling rate below ~900°C was such that a eutectic phase and needles developed, Figures 13c,13d and

14a.Figure 10 contains peaks from the SiC added MA steels which fit martensite rather than the ferrite recorded in the BM steel spectrum. This is particularly the case for the ~75μmMA steel. At the high cooling rates of the melt zone, austenite is not totally transformed to martensite and the phase outlining the boundaries in Figures 14b,14c and 14d may relate to the austenite, which is indicated in Figure 10 for MA ~75μm specimen. This proposed transformation sequence is supported by the XRD spectra. However, the XRD technique only allows identification of phases present above a minimum volume fraction, which does not preclude other phases such as Fayalite (Fe_2SiO_4) or Quartz (SiO_2), the latter recorded in Figures 15a-c,and those particularly within phase boundaries, which maybe iron silicides, present at levels below the detection limit of XRD. Also, because the XRD spectra were gathered from the MZ surface, while the EDX spectra were collected from a transverse cross-section of the MZ, the phases present may not match exactly. It is therefore possible that some of the peaks in Figure 10 are associated with phases having silicon contents greater than ~3 wt.%, shown by the EDX data in Tables 4 and 5. This is particularly the case for the peaks corresponding to the ordered phases of B2(FeSi) and DO_3(Fe_3 Si), which are known to form when the silicon content is higher than 5.4% [53,54]. DO_3(Fe_3 Si) is identified on Figure 10.B2(FeSi) shown as a small peak by Cava et al [53] is present in the same position on Figure10,just to the right of $FeSi_3$ at $2\theta = 65°$.Several of the XRD peaks in Figure 10 present in the spectra of both SiC incorporated steels,but particularly for the ~5μmSiC steel, match those of Cohenite, a mineral form of cementite.However, the SEM observations,for example Figures 13a and 13b, rarely conformed to the morphology of eutectic pearlite found in the BM.The various morphologies of the eutectic phase seen in this work were inhomogeneosly distributed throughout the MZ, and often adjacent to regions containing the needle phase.For example,another eutectic morphology, seen in Figure 18, was recorded from the middle of the MZ of ~5μm SiC MA steel,and has some characteristics of upper bainite and also degenerate pearlite; it will be

influenced by the local levels of carbon and silicon together with the cooling rate.The microhardness of these regions was ~550Hv compared to ~900Hv recorded for the needle areas.
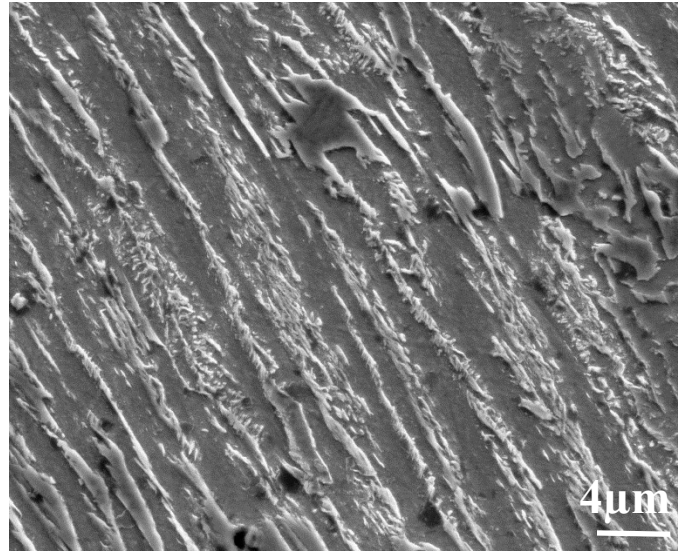

Fig.18.   Eutectic morphology in middle of MZ of ~5µm SiC MA steel.

Currently it therefore appears that the main contribution to the hardness levels presented in Figure 5, is due to the high volume fraction of martensite. According to Figure 19 taken from Bain [55], the hardness of an 0.12 -0.14%C martensite is about 300Hv.This means that the TIG melted zone with a hardness of ~800Hv, as seen in Figure 5,is associated with the presence of carbon martensites in the region of 0.5wt%,interspersed with other phases. This increase in carbon and silicon originates from the dissolution of SiC during the TIG processing [22,28]. The data in Table 4 gives an average Si of 2.03% for the ~5µm SiC MA steel, while Table 5 gives an average of 3.03% for the ~75µm SiC addition. If it is assumed that most of the silicon remains in solid solution in iron, this would provide hardening components of 16HV and 23HV [56]. These increases are insignificant compared with the effect of carbon. Also, silicon is known to promote the formation of graphite, the latter not adding significantly to the total hardness recorded in Figure 5.

As a result of this research, the surface engineering objective of achieving a significant increase in the hardness throughout a >1mm thick melted and solidified surface by dispersion hardening from an addition of silicon carbide particulates, is now considered to be due to the replacement of a ferrite –pearlite microstructure in the BM, by one with a high volume fraction of a martensite having a higher carbon content than the 0.2% of the BM. Also some graphite and retained austenite have been identified though the XRD spectra. A eutectic which is considered to include cementite is also present in some areas and will be investigated further. Silicon carbide particulates in this work are regarded therefore as a relatively economic source of carbon, which the TIG processing melts and disperses throughout the molten zone, aided by Marangoni flow [57].
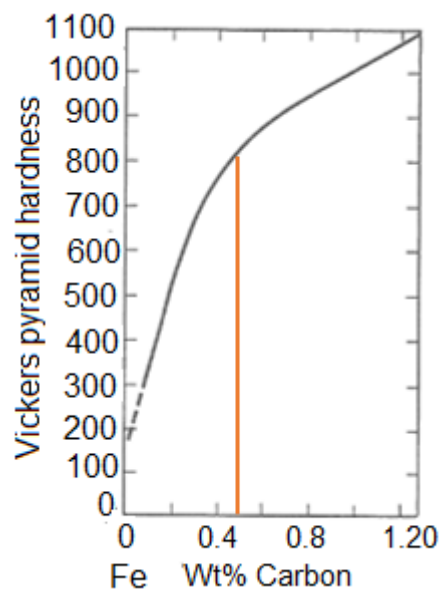
Fig. 19. Variation of VPH of martensite as a function of wt. % carbon [after ref.55]

5.Conclusions

Following the TIG processing of an 0.1wt.% C microalloyed steel preplaced with a paste of silicon carbide particulates of ~5μm or ~75 μm size at 0.3 mg mm^{-2}, a comparison was made of the effect of energy input on temperature, melt zone dimensions, wear rate, microhardness and microstructure of the single track surface region.

1.It was found that the temperature recorded by three thermocouples placed 5mm below the surface at 75mm, 150mm and 225mm from the start of processing, showed an increase of ~60% when the energy input was raised by 100% (from 210 J mm^{-1} to 420 J mm^{-1} or from 420 Jmm^{-1} to 840 J mm^{-1}).Compared with processing at 210 J mm^{-1}, processing at 420 Jmm^{-1} and 840 J mm^{-1} resulted in a significant increase in the volume of the melt zone together with corresponding increases in microhardness in a depth of >1mm, to a maximum of ~800Hv compared with 150Hv for the as- received MA steel plate.

2. Cracking was observed in the MZ following processing using 840 J mm^{-1}, but not at 420 Jmm^{-1}.

3.Following pin on disc wear testing, it was found that the steel incorporating the ~75μm size SiC particulates showed the highest CoF, but recorded the lowest wear rate over the ~10Km testing distance.

4.XRD and analytical SEM analyses showed that in the preplaced SiC steels, the dissolution of the particulates occurred, increasing both the carbon and silicon levels in the melt zone. In some regions of the ~75μm size SiC MA steel, this resulted in the formation of graphite, whilst the high cooling rate on solidification led to the transformation of most of the austenite to martensite, present in a variety of needle shapes. Also in other regions of the MZ, a eutectic phase was observed to be mixed with the needle phase. Some peaks in the XRD spectra of SiC MA steels were identified as Cohenite, a mineral form of cementite.

5.It is considered that martensite makes a significant contribution to the hardness recorded in the re-solidified melt zone.

6.In this research, the silicon carbide addition is regarded mainly as an economic source of carbon, which is dispersed throughout the melt zone giving rise to martensite mixed with a eutectic and other phases.

Acknowledgements

Disclosure statement

No potential conflict of interest was reported by the authors

References

1. Bach R, Damascheck E, Geissler E, Bergmann HW, Laser transformation of different steels, Proc.3rd European conf. on), In Bergmann HW, Kupfer R, editors. Laser Treatment of Materials (ECLAT'90). Coberg, Sprwechsaal Publishing Group; 1990.p. 265-282.

2. Song Y, Baker TN. A calorimetric and metallographic study of precipitation process in AA6061 and its composites. Mater Sci Eng A. 1995;201: 251-260.

3. Gurcan AB, Baker TN. Wear behavior of AA6061 aluminum-alloy and its composites. *WEAR*, 1995; 188**:** 185-191.

4. Daoud A, Abou El-khair MT. Wear and friction behavior of sand cast brake rotor made of A359-20vol%SiC particle composites sliding against automobile friction material. Tribo Internl. 2010; 43:544-553.

5. Rao RN, Das S. Effect of matrix alloy and influence of SiC particle on the sliding wear characteristics of aluminium alloy composites. Mater Des 2010; 31: 1200–1207.

6. Singh J, Chauhan A. Overview of wear performance of aluminium metal matrix conposities reinforced with ceramic material under the influence of controllable variables. Ceramics Internal.2016;42:56–81.

7. Shabani M-D, Paydar MH, Zamiri R, M. Goodarzi M, Moshksar MM. Microstructural and sliding wear behavior of SiC-particle reinforced copper matrix composites fabricated by sintering and sinter-forging processes. J Mater Res Technol.2016; 5:5-12.

8. Ion JC, Laser processing of engineering materials. Elsevier, Amsterdam,2005,261-326.

9. Zhong M, Liu W. Laser surface cladding: the state of the art and challenges. Proc. Inst. Mech. Eng. Part C. J Mech Eng Sci. 2010; 224:1041-1062.

10. Baker TN. Laser surface modification of titanium alloys in Surface engineering of light alloys, Dong H, editor, Woodhead Publishing; 2010.p.398-443.

11. Ayers JD, Schaefer RJ, Proc. conf. Laser applications in material processes, Ready JF, editor, Bellingham, SPIE, 1979; p. 57- 64**.**

12. Ayers JD, Tucker TR. Particulate-TiC-hardened steel surfaces by laser melt injection. Thin solid films, 1980;73:201-207.

13. Ayers JD, Schaefer RJ, Robey WP. A laser processing technique for improving the wear-resistance of metals. J Met1981; 33:19-23.

14. Ayers JD, Bolster RN. Abrasive wear with fine diamond particles of carbide-containing aluminum and titanium-alloy surfaces. Wear. 1984; 93:193-205.

15. Mridha S, Baker TN. Metal matrix composite layer formation with 3 mu SiCp powder on IMI318 titanium alloy surfaces through laser treatment. J Mater Proc Technol.1997; 63: 432-437.

16. Archard JF, Hirst W. The wear of metals under unlubricated conditions. Proc Roy Soc Lond. 1956; 236A:397-410.

17. Abboud JH, West DRF. Microstructure of titanium injected with SiC particles by laser processing. J Mater Sci Lett. 1991; 10:1149-1152.

18. Baker TN, Xin H, Hu C, Mridha S. Design of surface in-situ metal-ceramic composite formation via laser treatment. Mater SciTechnol.1994; 10: 536-544.

19. Mridha S, Baker TN. Metal matrix composite layers formed by laser processing of commercial purity Ti-SiCp in nitrogen environment. Mater Sci Technol.1996;12: 595-602.

20. Hu C, Barnard L, Mridha S, Baker TN. The role of SiC particulate and Al2O3 (Saffil) fibers in several alloys during the formation of in situ MMCs developed by laser processing. J Mater Proc Technol.1996;58:87-95.

21 Terry B, Chinyamakobvu OS. Assessment of the reaction of SiC powders with iron-based alloys. J Mater Sci. 1993; 28:6779-6784.

22. Pelleg J. Reactions in the matrix and interface of Fe-SiC metal matrix composite system. Mater Sci Eng. 1999; A269: 225-241.

23.Gemelli E, Gallerie A, Caillet M. Improvement of resistance of oxidation by laser alloying on a tool steel surface. Scr Mater.1998; 39: 1345–1352.

24. Čikara D, Rakin M, Todic´ A. Cast steel–SiC composites as wear resistant materials. FME Trans. 2009; 37: 151–155.

25. Zhang C, Pei S, Ji H, Cui Y, Li M. Fabrication of Ni60–SiC coating on carbon steel for improving friction, corrosion properties. Mater Sci Technol. 2017; 33:446-453.

26. Majumdar JD, Chandraa BR, Nath AK, Mannaa I. Studies on compositionally graded silicon carbide dispersed composite surface on mild steel developed by laser surface cladding. J Mater Proc Technol. 2008; 203:505–512.

27. Mridha S, Ng B. Addition of ceramic particles to GTAW melted titanium surfaces. Surf Eng. 1999; 15: 210-215.

28. Buytoz S. Microstructural properties of SiC based hardfacing on low alloy steel Surf Coat Technol.2006; 200:3734– 3742.

29.Reddy GS, Arul S, Sellamuthu R. Improving surface hardness of mild steel plates by addition of silicon carbide using gas tungsten arc as heat source. Appl Mech Mater. 2014;592-594: 879-882.

30. Patel P, Mridha S, Baker TN. Influence of shielding gases on preheat produced in surface coatings incorporating SiC particulates into microalloy steel using TIG technique. Mater Sci Technol. 2014; 30:1506-1514.

31. Muñoz-Escalona P, Mridha S, Baker TN. Effect of Shielding Gas on the Properties and microstructure of melted steel surface TIG Torch. Advan Mater Proc Technol. 2015; 1:435-443.

32.Information on http://net.grundfos.com/doc/webnet/mining/downloads/pump-handbook.pdf.

33. Information on http://www.in-situ.co.uk/crankshaft-machining.

34. Choi Y, Liu R. Performance of nano/micro CBN particle coated tools in superfinish hard machining. Int J Mac Tools Manuf. 2009; 49: 683-689.

35. Uhlman E, Oyane del Fuentes JA, Keunecke M. Machining of high performance workpiece materials with CBN coated cutting tools. Thin Solid Films. 2009; 518: 1451-1454.

36. Information on http://www.welding-consultant.com/WeldCracks.pdf

37.Muñoz de Escalona P, Mridha S, Baker TN. Effect of silicon carbide size particle on the properties and microstructure of melted steel surface using TIG torch. Adv Mater Proc Technol. 2016; 2: 451-460.

38.Easterling KE. Introduction to Physical Metallurgy of Welding, 1992, Butterworth-Heinemann, London.

39. Rasool G, Stack MM. Wear maps for TiC composite based coatings deposited on 303 stainless steel. Tribo Int. 2014; 74: 93–102.

40.Hu C, Baker TN. The importance of preheat before laser nitriding a Ti-6Al-4V alloy. Mater Sci Eng A. 1999;265: 268-275.

41. Kotecki D J, Cheever DL, Howden DG. Mechanism of Ripple Formation During Weld Solidification. Weld J,1972;51:386S-391S.

42. Kou S, Limmaneevichitr C, Wei P S. Oscillatory Marangoni Flow: A Fundamental Study by Conduction-Mode Laser Spot Welding. Weld J. 2011; 90:229S-240S.

43. Pei YT, Ouyang JH, Lei TC, Zhou Y. Microstructure of laser-clad SiC-(Ni alloy) composite coating. Mater Sci. Eng.1995;194A 219-224.

44. Tewari SP, Gupta A, Prakash J. Effect of welding parameters on the weldability of material. Internal J Eng Sci Technol. 2010;2: 512-516.

45. https://hypertextbook.com/facts/2005/steel.shtml

46. Ghosh PK, Kumar R. Surface modification of micro-alloyed high strength low alloy steel by controlled TIG arc process. Metall.Mater.Trans.A 2015;46A:831-842.

47. Mridha S, Baker T N. Crack-free hard surfaces produced by laser nitriding of commercial purity titanium. Mater Sci Eng. 1994; A188:229-239.

48. DePond PJ, Guss G, Ly S, Calta NP, Deane D, Khairallah S, Matthews MJ. In situ measurements of layer roughness during laser powder bed fusion additive manufacturing using low coherence scanning interferometry, Mater. Des.2018; 154: 347–359.

49. Tang W M, Zheng ZX, Ding HF, Jin ZH. A study of the solid state reaction between silicon carbide and iron. Mater Chem Phys.2002;74: 258-264.

50. Kawanishi S, Yoshikawa T, Tanaka T. Equilibrium phase relationship between SiC and a liquid phase in the Fe-Si-C system at 1523-1723K. Mater. Trans.2009; 50:806-813.

51. Runnsjö G. On the accuracy of carbon determinations in steels by electron probe microanalysis. Scan. J Metall.1980; 9:199-203.

52. Goldstein J I, Newbury D E, Echlin P, Joy D C, Fiori C, Lifshin E. Scanning Electron Microscopy and X-ray microanalysis. Plenum Press, New York, London,1984.

53. Cava RD, Botta WJ, Kiminami CS, Olzon-Dionysio M, Souza SD, Jorge Jr. AM, Bolfarini C. Ordered phases and texture in spray-formed Fe–5wt%Si. J Alloys Compds.2011; 509S:S260-264.

54. Jang P, Choi G. Effects of Silicon Content on the Properties of Gas-Atomized Fe–Si–Cr Powders. IEEE Trans Mag.2017;53: 2002705.

55. Bain E C. Functions of alloying elements in steels.ASM, Cleveland,1939.

56.Pickering FB, Gladman T. An investigation into some factors which control the strength of carbon steels', in 'Metallurgical developments in carbon steels', Sp. Report 81, ISI, London,UK,1963,11-20.

57. Mills KC, Keene BJ, Brooks RF, Shirali A. Marangoni effects in welding. Proc. R. Soc. London A1998; 356A: 911–925.